Atmos. Chem. Phys., 10, 6627–6644, 2010
www.atmos-chem-phys.net/10/6627/2010/
doi:10.5194/acp-10-6627-2010

Atmospheric Chemistry and Physics

Characterization of particle cloud droplet activity and composition in the free troposphere and the boundary layer during INTEX-B

G. C. Roberts[1], D. A. Day[1], L. M. Russell[1], E. J. Dunlea[2], J. L. Jimenez[2,3], J. M. Tomlinson[4,*], D. R. Collins[4], Y. Shinozuka[5,], and A. D. Clarke[5]**

[1]Scripps Institution of Oceanography, University of California, San Diego, La Jolla, CA, USA
[2]Cooperative Institute for Research in the Environmental Sciences (CIRES), Boulder, CO, USA
[3]Department of Chemistry and Biochemistry, University of Colorado, Boulder, CO, USA
[4]Department of Atmospheric Sciences, Texas A&M University, College Station, TX, USA
[5]School of Ocean and Earth Science and Technology, University of Hawaii, Honolulu, HI, USA
[*]now at: Pacific Northwest National Laboratory, Richland, WA, USA
[**]now at: NASA Ames Research Center, Moffett Field, CA, USA

Received: 14 January 2010 – Published in Atmos. Chem. Phys. Discuss.: 9 February 2010
Revised: 17 June 2010 – Accepted: 17 June 2010 – Published: 20 July 2010

Abstract. Measurements of cloud condensation nuclei (CCN), aerosol size distributions, and submicron aerosol composition were made as part of the Intercontinental Chemical Transport Experiment Phase B (INTEX-B) campaign during spring 2006. Measurements were conducted from an aircraft platform over the northeastern Pacific and western North America with a focus on how the transport and evolution of Asian pollution across the Pacific Ocean affected CCN properties. A broad range of air masses were sampled and here we focus on three distinct air mass types defined geographically: the Pacific free troposphere (FT), the marine boundary layer (MBL), and the polluted continental boundary layer in the California Central Valley (CCV). These observations add to the few observations of CCN in the FT. CCN concentrations showed a large range of concentrations between air masses, however CCN activity was similar for the MBL and CCV ($\kappa \sim 0.2$–0.25). FT air masses showed evidence of long-range transport from Asia and CCN activity was consistently higher than for the boundary layer air masses. Bulk chemical measurements predicted CCN activity reasonably well for the CCV and FT air masses. Decreasing trends in κ with organic mass fraction were observed for the combination of the FT and CCV air masses and can be explained by the measured soluble inorganic chemical components. Changes in hygroscopicity associated with differences in the non-refractory organic composition were too small to be distinguished from the simultaneous changes in inorganic ion composition in the FT and MBL, although measurements for the large organic fractions (0.6–0.8) found in the CCV showed values of the organic fraction hygroscopicity consistent with other polluted regions ($\kappa_{org} \sim 0.1$–0.2). A comparison of CCN-derived κ (for particles at the critical diameter) to H-TDMA-derived κ (for particles at 100 nm diameter) showed similar trends, however the CCN-derived κ values were significantly higher.

Correspondence to: G. C. Roberts
(gcroberts@ucsd.edu)

1 Introduction

Single variable parameterizations simplify estimates of cloud condensation nuclei (CCN) concentrations in climate models; yet their application to a range of aerosol types is still not well characterized. It has long been known that estimating CCN concentrations based on the measured size distribution and an assumed pure salt composition (ammonium sulfate) often leads to an over-prediction of CCN concentrations (e.g., Bigg, 1986). Roberts et al. (2002) use size-resolved chemical composition measured by MOUDI during

the wet season in the Amazon Basin and show that, within the limits of expected solubility of organics, predicted and observed CCN were in agreement. Their results suggested that CCN activity can be predicted with a simplified binary aerosol composition of a water soluble and insoluble species. Chang et al. (2007) show that for a rural location they could predict the CCN within 15% by using size-resolved measurements obtained with aerosol mass spectrometry (AMS) and assuming that all organic mass was insoluble. They demonstrate that using bulk composition measurements for predicting CCN resulted in poorer correlations and a 30% systematic offset. Chang et al. (2007) and Wang et al. (2008) show that when organics dominate the aerosol mass, the composition of the organic fraction becomes more important for estimating CCN activity. A similar comparison using AMS measurements was reported for a recent study conducted in the Amazon Basin (Gunthe et al., 2009). Their results show that the best predictions of CCN concentrations are achieved with highly time-resolved calculations of κ (a single variable hygroscopicity parameter, κ; Petters and Kreidenweis, 2007) based on individual observations of size-resolved chemistry and aerosol size distributions. While Gunthe et al. (2009) show that predictions of CCN concentrations using the bulk AMS mass resulted in similar concentrations to those observed, the predictions based on an average hygroscopicity parameter were less accurate. Rose et al. (2010) conclude that a constant hygroscopicity parameter (κ=0.3) is adequate for estimating CCN activity of continental aerosols in large scale climate models. They do note, however, that constant κ does not capture temporal variations of CCN concentrations that would be used in models with shorter timescales. These results and other recent studies (Andreae, 2009; Jimenez et al., 2009; Sullivan et al., 2009) suggest that aerosols from various sources undergo atmospheric processes that tend to homogenize their chemical and physical properties with respect to CCN activity.

The Intercontinental Chemical Transport Experiment – Phase B (INTEX-B) campaign was designed to investigate the effects of transport and evolution of Asian pollution and how it impacts air quality and climate in western North America (Singh et al., 2009). It has been shown that during spring pollution plumes originating in Asia are rapidly transported across the Pacific (3–5 days), transporting dust (Stith et al., 2009), other particles, and trace gases (Cooper et al., 2010) to the North American Continent. Aircraft and satellite measurements and modeling conducted as part of INTEX-B provided extensive evidence of trans-Pacific pollution transport during the campaign (Singh et al., 2009 and references therein). Prior to INTEX-B, Roberts et al. (2006) present measurements of CCN over the eastern Pacific (during the Cloud Indirect Forcing Experiment, CIFEX) and provide a comparison of predicted CCN activity for different air mass categories characterized by aerosol size distributions and air mass history. For the MILAGRO/INTEX-B aircraft campaigns, Shinozuka et al. (2009) investigated the links between submicron organic mass fraction and CCN activity and optical properties in the free troposphere to assess the viability of predicting aerosol composition and thus CCN activity using remote sensing measurements.

In this study, we observe differences in CCN activity for three main classes of air masses sampled during INTEX-B and focus on the relationships between the physicochemical properties, in particular organic composition, and CCN activity, and discuss the atmospheric processes that may lead to the observed CCN properties. Distinctly different air masses were sampled within the free troposphere above the Pacific, in the marine boundary layer, and in the polluted continental boundary layer, which provided a unique opportunity to investigate CCN activity over a large range of chemical composition and atmospheric history. We also explore the relationship between κ and aerosol chemistry to assess chemical transformations related to atmospheric processes.

2 Experimental methods

Measurements discussed in this manuscript were made during the Intercontinental Chemical Transport Experiment – Phase B (INTEX-B) from the NCAR C130 aircraft during April and May 2006. The aircraft was based at Paine Field in Everett, Washington, which is ca. 35 km north of Seattle. Twelve flights were conducted, all based at Paine field except the ferry fights bracketing the study between Colorado and Washington. The majority of the flight time was in the free troposphere above the eastern Pacific or western Washington, Oregon, and California with the primary goal to intercept trace gas and aerosol pollution layers transported across the Pacific Ocean. Typical flight duration was seven to eight hours, spanning altitudes of 100 m to 7500 m above sea level (m a.s.l.). In addition to profiles of the free troposphere, some flights included legs in and just above the boundary layer over the Pacific Ocean, Seattle metropolitan area, and the California Central Valley. Figure 1 shows a map of the region of study with flight tracks indicating the location of sampling periods that are the focus of this analysis. The instruments that were used in this study for the analysis presented here are described in the sub-sections below. All CCN and aerosol number concentrations reported during this study are for ambient temperatures and pressures. Aerosol particles were collected on the C130 through the University of Hawaii (UH) solid diffuser inlet. Previous characterizations of this inlet indicate a 50% cut-off aerodynamic diameter (D_{50}) of 5 µm (McNaughton et al., 2007).

2.1 Measurements

2.1.1 Continuous flow streamwise thermal-gradient CCN instrument

Cloud condensation nuclei concentrations were quantified using a continuous flow streamwise CCN instrument

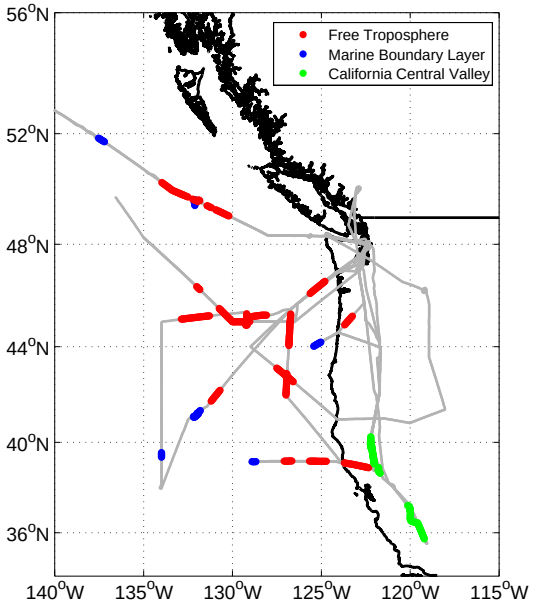

Fig. 1. Flight tracks for each level leg used in analysis. Tracks are color-coded by air mass category: free troposphere (red), marine boundary layer (blue), and continental boundary layer (green). Grey lines indicate entire flight tracks for each research flight included in this analysis.

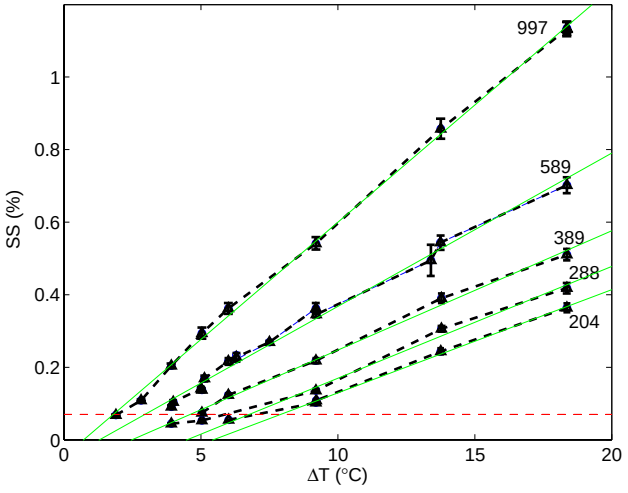

Fig. 2. Calibration of DMT-CCN instrument as a function of temperature gradient at different pressures (units: mbar). Green lines are best fits through the data. The red dashed-line represents 0.07% supersaturation (the lower operating limit of the CCN chamber, Roberts and Nenes, 2005).

(CF-CCN; Droplet Measurement Technologies, Boulder, CO). CCN concentrations were measured with a continuous flow (0.5 L/min) and constant temperature difference (5 °C). Briefly, the CF-CCN exploits the differences in diffusion of heat and water vapor to maintain a quasi-uniform supersaturation along the streamwise axis of the chamber. The chamber consists of a vertical cylindrical column, with wetted surfaces that are exposed to a temperature gradient oriented with the flow along the vertical axis. Droplets that grow to larger than 1.0 µm diameter are considered CCN and used to measure the CCN concentration. CCN counting is continuous and the time resolution is only limited by the precision of single particle counting statistics. The instrument and application has been described in detail by Roberts and Nenes (2005), Lance et al. (2006), and Rose et al. (2008).

During this campaign, no constant pressure controller was used at the inlet of the CCN chamber, which means the supersaturations vary with altitude from ∼0.3% near the surface to ∼0.1% at higher altitudes (∼7500 masl). Only data during straight and level parts of the flights were used because of changes in CCN instrument saturation ratios during ascents and descents of the aircraft. The automated analysis routine removed ascent and descent data that averaged more than 1.5 mbar min^{-1} during a 60-s period. The calibration of the CCN instrument at different pressures and temperature gradients is shown in Figs. 2 and 3. The calibrations were performed in the laboratory using ammonium sulfate aerosol at temperature differences between 2 and 18 °C and internal chamber pressures between 200 and 1000 mbar. While the relationship between supersaturation, temperature gradient and pressure are linear within the operating limits of the instrument (Roberts and Nenes, 2005), these relationships are only valid for level flight legs. The experimentally-derived expression to calculate the supersaturation is given by:

$$m_P = a_m P + b_m; a_m = 5.087\text{e}^{-5}; b_m = 1.833\text{e}^{-2} \quad (1)$$

$$y_P = a_y P + b_y; a_y = 1.429\text{e}^{-4}; b_y = -0.1747 \quad (2)$$

$$S = m_P \times \Delta T + y_P \quad (3)$$

where P is chamber pressure (mbar), ΔT is top-to-bottom column temperature difference (°C), and m_P and y_P are functions of CCN chamber pressure, and are used to calculate the supersaturation, S, based on ΔT. This calibration employs a constant van't Hoff factor of 2.52 (Rose et al., 2008) and allows the calculation of supersaturation to within 10% 1-sigma deviations (Fig. 2) for CCN columns with similar dimensions to those developed by Droplet Measurement Technologies at a 0.5 liter per minute (lpm) flow rate. The above expression agrees to within 10% of supersaturations for conditions reported in Rose et al. (2008). Dry critical activation diameters were determined automatically using an algorithm that determines the inflection point of the activation curves (i.e., the diameter where the slope in the relationship between the activated fraction and mobility diameter is highest). At lower supersaturations (Sc<0.2%), the activation curves broaden which reduced the accuracy at which the automatic routine determined the critical diameter, contributing to the greater variability between predicted and observed

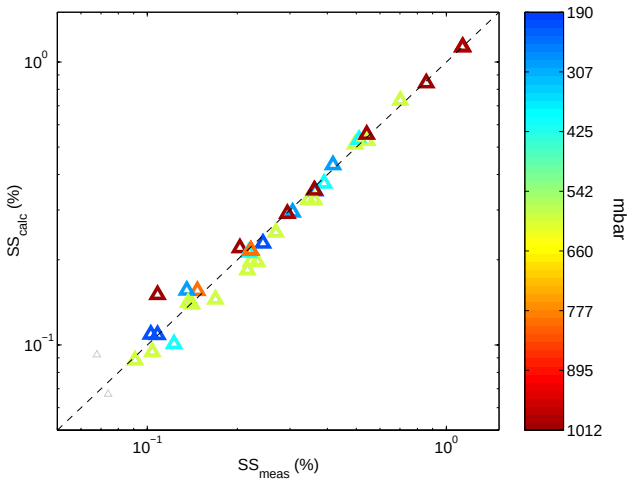

Fig. 3. Comparison of calculated and measured supersaturations based on calibrations in Fig. 2 (r^2=0.96). Markers are color coded for pressure at which the calibrations were performed.

supersaturations observed in Fig. 3. More precise calibrations in future studies using this instrument (i.e., higher resolution activation curves, multiple charge corrections, well-calibrated flow rates and temperature sensors) should further reduce the uncertainty to less than 10%.

The CCN observations were compared to the measurements of aerosol size distributions to determine the critical dry diameter at which the aerosol is cloud active. This comparison assumes that particles of a given size have a uniform composition, where diameter can be related to the water-soluble fraction and expressed as a single parameter approximation. We have used the κ-Köhler approximation in this study (Petters and Kreidenweis, 2007); a discussion of the different single-parameter approximations is also found in Gunthe et al. (2009). These single-parameter approximations assume negligible surface tension effects to empirically determine the water activity of the material in the particle. We report critical diameter, d_{pc}, and κ here. As we only measure CCN concentrations at a single supersaturation in order to obtain 1 Hz measurements for enhanced spatial resolution onboard the C130, we use the derived chemical information (implicit in κ) to compare to independent observations of aerosol chemistry for different air mass types.

CCN spectra were computed in this study using size distributions measured by SMPS (Sect. 2.1.2) and bulk submicron chemical composition measured by AMS and SP2 (Sect. 2.1.3). Since the flight legs during INTEX-B were generally short and the mass concentrations were typically low, size-resolved AMS chemical composition cannot be effectively used for most of this study due to the low signal-to-noise. Hence, CCN activity based on the bulk aerosol chemistry (~0.04–0.7 µm physical diameter) is used; however, we emphasize that bulk chemistry clearly biases the CCN concentrations based on aerosol chemistry at larger sizes (several hundred nm) where particles are more massive but contribute less to the number concentration at the diameters around 100 nm which are at the fence of CCN activation (Gunthe et al., 2009). Cases ranging from pure ammonium sulfate (κ=0.61) to nearly insoluble particles (κ=0.01) are shown to provide a reference. Table 2 describes the properties of the chemical components used to calculate the CCN activity based on a simplified Köhler equation (Köhler, 1936; Shulman et al., 1996).

For the inorganic non-refractory components, the ammonium was first assigned to nitrate to determine the ammonium nitrate (AN; generally small accept in polluted boundary layer), and the remaining ammonium determined the relative contributions of ammonium sulfate (AS), ammonium bisulfate (ABS), and sulfuric acid (SA). Organic matter was approximated as insoluble and CCN-inactive. Limiting cases were calculated by assigning the non-chemically resolved mass to either dust or NaCl. We test these assumptions in this manuscript and report on their viability in the Results and Discussion sections.

2.1.2 Aerosol size distributions

Size distributions were measured by two research groups on the C-130 during INTEX-B. We used both datasets in this analysis to maximize the number of level flight legs available for comparison with CCN observations. Size distributions from 13 nm to 750 nm using a differential mobility analyzer (DMA) were measured with a 90s scan time (Tomlinson et al., 2007; Texas A&M University, TAMU). Aerosol size distribution measurements (10 nm$<D_p<$10 µm) were also recorded by the Hawaii Group for Environmental Aerosol Research (HiGEAR). HiGEAR size distributions comprise measurements from a radial differential mobility analyzer (rDMA), an optical particle counter (OPC) and an aerodynamic particle sizer (APS). Measurements from the three instruments were performed at constant relative humidity (RH~30%) and were merged onto the closest 1-minute timestamp. rDMA samples were collected over 20-s periods into a lagged aerosol grab chamber for subsequent analysis (Clarke et al., 1998). The size distributions quantified with the HiGEAR rDMA (10–250 nm diameter) and the TAMU DMA were both corrected for sampling line losses, bipolar charging probabilities, transfer functions (diffusion broadening and losses) and particle counting efficiencies (Zhou et al., 2002). The OPC sizes (150 nm–5 µm; 3-s averaging time) were calibrated with polystyrene latex spheres and not corrected for ambient aerosol refractive indices. The APS sizes (3–10 µm diameter) were adjusted for an assumed density of 1.8 g cm^{-3} and not corrected for transmission loss. Further details on the HiGEAR particle sizing instrumentation except for the APS is provided in Shinozuka et al. (2009). The integrated number concentration of the HiGEAR merged size distribution dataset (SMPS-OPC-APS) was scaled to

independently measured CPC number concentrations (CPC; Model 3010, TSI; average scaling: +15±14%). The scaled HiGEAR size distributions agreed well with integrated total number concentrations measured by TAMU for legs within the free troposphere. However, agreement in integrated number concentrations between both sets of size distributions was poor (ca. factor of two difference) when the majority of the particle number concentration was contained within a smaller aerosol mode ($Dp < 20$ nm) such as in the polluted continental boundary layer or marine boundary layer. The HiGEAR size distributions were only scaled to the concurrent CPC measurements for observations in the free troposphere. Observations within the MBL (during RF2 only) were adjusted by the average difference between HiGEAR integrated number concentration and CPC concentrations in the free troposphere (an increase of 15%). Application of these adjustments produced comparable results for calculations of critical diameters and hygroscopicity parameters using either the TAMU or HiGEAR size distributions. Size-resolved particle hygroscopicity was measured with a humidfied tandem differential mobility analyzer (H-TDMA) of Texas A&M University (Gasparini et al., 2004; Tomlinson et al., 2007). Dry classified particles (RH<5%) of 50, 100, 200 and 300 nm diameter were exposed to an elevated RH at 84%; a second DMA measured the hygroscopic growth of the particles. The resulting hygroscopic growth factors are used to determine H-TMDA-derived kappas, which are compared to CCN-derived kappas in Sect. 4 (Discussion).

2.1.3 Aerosol mass spectrometer and single-particle soot photometer

Submicron aerosol composition measurements were made using an Aerodyne High-Resolution Time-of-Flight Aerosol Mass Spectrometer (HR-ToF-AMS) (DeCarlo et al., 2006). A detailed description of the operation of the AMS on board the C130 is described by DeCarlo et al. (2008) and further details specific to INTEX-B are described in Dunlea et al. (2009). The AMS provided bulk concentrations (organics, sulfate, nitrate, ammonium, and chloride) for time intervals of 12 s. Since the AMS detects only species that evaporate from the aerosol at 600 °C under high vacuum, the subset of aerosol components detected by the AMS is named non-refractory (NR). Therefore, refractory material such as crustal minerals (dust), soot, and some salts (e.g. NaCl) are not detected. The AMS concentrations have been compared to those determined from the SMPS, a particle-into-liquid sampler, and an independent comparison method with light scattering measurements as described by DeCarlo et al. (2009) (Fig. 2 and associated discussion) and Dunlea et al. (2009) (Figs. 2 and 3 and associated discussion). The comparisons show consistent quantification of the AMS data, which is more obvious at the higher signal levels of Mexico City where the effect of noise in all the measurements is lower (DeCarlo et al., 2009). During this study, black carbon mass was measured with a Single Particle Soot Photometer (SP2) instrument (DMT, Boulder, CO) as described in Subramanian et al. (2010), and typically represented a few percent of the NR mass. In addition, dust and sea salt particle mass contributions are expected to be small in the size range of interest for CCN closure (∼50–200 nm). Albeit always a small contribution to submicron aerosol mass, we include the BC measurements in this analysis and thus assume any chemically unresolved submicron components are either dust or salts. The NR organic mass fraction (nrOMF) is the ratio of the bulk organic mass measured by AMS to the mass estimated using the integrated submicron SMPS size distributions using a density approximated from the NR components (PM_1). The NR inorganic mass fraction (nrIMF) is calculated as the ratio of the bulk inorganic mass to the estimated PM_1 mass. The AMS instrument was operated continuously alternating between the "Mass Spec" (MS) mode which yields bulk chemical information and the "Particle Time-of-Flight mode" (PToF) mode that allows for particle sizing and size distribution measurements (Jimenez et al., 2003), and which ToF-AMSs can perform at all *m/z* in the spectrum (DeCarlo et al., 2006). In this analysis we use the higher sensitivity MS mode data for calculations of CCN activity using bulk chemical information; as discussed above, the signal-to-noise of the size-resolved measurements was not sufficient for most of our analyses. Detection limits at STP (273 K, 1 atm) for 12 s data were 0.35 μg sm^{-3} for organics and ammonium, and 0.05 μg sm^{-3} for sulfate, nitrate, and chloride (Dunlea et al., 2009). Detection limits scale with the square-root of the averaging time (Drewnick et al., 2009), therefore for 90-s and 10-min averaging periods detection limits of organic mass and ammonium were 0.13 and 0.05 μg sm^{-3} and detection limits for sulfate, nitrate, and chloride were 0.018 and 0.007 μg sm^{-3}, respectively. Chloride concentrations were nearly always below the detection limit and are not discussed here. Concentrations reported are in units of μg m^{-3} at ambient temperature and pressure.

Oxygen-to-carbon ratios (O/C) for organics were estimated from the high-resolution mass spectra according to the techniques developed by Aiken et al. (2007, 2008). This method of deriving O/C has an estimated accuracy for individual species of ±31%. In the HR-ToF-AMS the elemental compositions of most mass fragments at the same integer *m/z* can be unequivocally assigned, which forms the basis of the elemental composition determination when the elemental concentrations contained in all detectable mass fragments are summed, followed by an empirical correction to account for fragmentation biases (Aiken et al., 2007, 2008). AMS Mass fragment *m/z* 44 typically arise from carboxylic acids functional groups, which are expected to comprise a large fraction of oxygenated aerosol (Heald et al., 2010). However, other oxygenated functional groups such as alcohols may contain a significant fraction of oxygenated functional groups and do not produce a large *m/z* 44 signal. It has been shown that O/C ratios can be derived by using the ratio of the AMS *m/z*

44 mass fragment to the total organic signal and agree with ±9% with O/C calculated with the high-resolution spectra (Aiken et al., 2008). O/C ratios used in this analysis were calculated using the AMS *m/z* 44 to total organic ratio and showed agreement within ±9% with the high-resolution O/C calculations done in Dunlea et al. (2009) for select flights. Therefore, for O/C reported here, we represent the expected error by adding in quadrature the theoretical error (±31%), the error related to using the *m/z* 44 fragment (±9%), and the instrument precision for each flight leg (root mean square).

2.1.4 Scanning transmission X-ray microscopy

Single particles were collected on Si_3N_4 windows and analyzed using scanning transmission X-ray microscopy-near edge X-ray absorption fine structure spectroscopy (STXM-NEXAFS). Transmission of photons at energy levels between 278 and 320 eV was measured over a minimum spatial resolution of 30 nm and converted to optical density using a protocol described by Russell et al. (2002). Spectra were then classified according to the presence and relative absorbance intensities of organic functional groups (alkyl, ketonic, carboxylic carbonyl, alkene, and aromatic), carbonate, and potassium. Particles were also categorized as having a "spherical" or "irregular" morphology. Details of the spectral and image classification methods are described in Takahama et al. (2007). During INTEX-B, 113 particle spectra were obtained from 10 locations. Each of the spectra from the individual particles were classified into one of the 14 categories established by Takahama et al. (2007). Furthermore, several of the 14 spectra types were categorized into one of four metaclasses – Secondary, Biomass, Ultisol (pine ultisol; a red clay soil), and Combustion, determined by similarity to spectra of samples with known composition in the published literature. The STXM analysis allows qualitative confirmation of aerosol sources including combustion and urban emissions. Additionally, non-spherical particles in the supermicron range may be indicative of the presence of dust. Day et al. (2009) presents further details on the single particle collection and analysis with STXM-NEXAFS during INTEX-B. Here we present single particle STXM measurements as evidence for long-range transport.

2.1.5 Back trajectories

Back trajectories point to long-range transport of pollution layers across the Pacific Ocean and some case studies have been discussed previously (e.g. Dunlea et al., 2009); however, the sampling in these layers during horizontal legs was a relatively small fraction of the experiment. Therefore, our observations focus on characterizing CCN and aerosol properties in the three major types of air masses observed during this experiment: free troposphere above the Pacific Ocean (FT), marine boundary layer (MBL), and California Central Valley (CCV). Our analysis uses 7-day kinematic back trajectories compiled by the Fuelberg research group at Florida State University (http://fuelberg.met.fsu.edu/research/intexb/) to infer origin and atmospheric processes associated with each air mass. Typically 15–30 trajectories were calculated at equally spaced time intervals during each level leg to give a broad perspective of the likely source regions of the air mass. All of the trajectories for legs flown in the MBL indicated that the air mass was not recently affected by the N. American continent and generally originated in the north Pacific, sometimes indicating contact with northeastern Siberia or Alaska several days earlier. Most of the trajectory ensembles for legs flown in the free troposphere above the Pacific were associated with similar trajectories, with the majority for each flight leg originating in East Asia 3–5 days prior to sampling. Two legs in the free troposphere showed back trajectories that were transported from the mid-Pacific, with possible vertical mixing that incorporated marine boundary layer air, but having no evidence of contact with North America or Asia. Back trajectories were not used for analysis of California Central Valley samples as regional pollution clearly dominates aerosol in the boundary layer. Table 1 summarizes the level legs discussed here, including both the sample location classification (FT, MBL, CCV) and the air mass origin as indicated by back trajectories: "Long Range Transport", "Pacific", and "North American". All level legs flown in the California Central Valley boundary layer are classified as North American.

3 Results

In this section, we discuss CCN results grouped by the three major categories of air masses discussed above: free troposphere (FT), marine boundary layer (MBL), and the polluted continental boundary layer. Measurements in the continental boundary layer were taken in California Central Valley (CCV) during INTEX-B – we select these measurements to represent a polluted urban aerosol. Air mass categories are similar to those discussed in Dunlea et al. (2009), except that our criteria for FT is less strict than theirs (which was west of −125 W), and included flight legs slightly inland (<100 km; at >2300 m altitude) The analysis presented here also does not differentiate between FT and Asian-influenced FT by the same definition described in Dunlea et al. (2009), as the two air mass categories were separated by sulfate loading greater or less than 1 μg SO_4 m^{-3}, respectively. This distinction was not used in this manuscript since few of the FT air masses included in this analysis fit that criterion. The Dunlea et al. (2009) analysis additionally included air masses in the Seattle region (excluded here) and does not include the additional category of MBL. Results are presented as averages for level flight legs of duration 5–30 min. Table 1 summarizes the dates, altitude ranges, duration, sample location and air mass origin for the level legs included in this analysis. The flight tracks for the data presented in Table 1 are shown

Table 1. Summary of altitude ranges, air mass locations and origins for flight legs analyzed.

Flight	Sample Location	Altitude Range (m)	# Legs	Air Mass Origin Time (min)	Total Measurement
RF02	FT	3500–6800	4	Long Range Transport	57
21 Apr 2006	MBL	610–720	2	Pacific	18
RF04	FT	5000–5600	2	Pacific	24
26 Apr 2006					
RF05	FT	3100–5500	6	Long Range Transport	34
28 Apr 2006	MBL	390–530	2	Pacific	11
RF07	CCV	550	4	North America	35
3 May 2006					
RF09	FT	5500–5600	3	Long Range Transport	26
8 May 2006	MBL	100	1	Pacific	4
	CCV	480-500	2	North America	33
RF10	FT	4400	1	Long Range Transport	14
9 May 2006					
RF11	FT	2300–4300	5	Long Range Transport & Pacific	48
11 May 2006	MBL	170	1	Pacific	6
	CCV	500	1	North America	9

Table 2. Properties of components used to estimate CCN activity.

Component	Density ($g\ cm^{-3}$)	Molecular Wt. $g\ mol^{-1}$	Solubility $g\ ml^{-1}\ H_2O$	van't Hoff factor –
$(NH_4)_2SO_4$	1.77[a]	132.13	0.764	2.52[d]
$(NH_4)HSO_4$	1.78[a]	115.11	–	3
H_2SO_4	1.84[a]	98.08	–	3
$(NH_4)NO_3$	1.72[a]	80.04	0.150	2
NaCl	2.165[a]	96.06	0.359	2
Dust	NA	NA	0	0
Black Carbon	1.9[b]	NA	0	0
Insoluble Organic	1.4[c]	NA	0	0

[a]Lide (2010); [b] Bond and Bergstrom (2006); [c] Hallquist et al. (2009); [d] Rose et al. (2008a).

in Fig. 1. Table 3 includes the physical properties of the dominant mode of the aerosol size distribution that contributed to CCN concentrations and Table 4 shows the chemical mass composition of submicron particles analyzed by AMS. All means and standard deviations reported in Tables 3 and 4 were calculated from single averages determined for each flight leg analyzed and classified as a particular air mass type. Arithmetic means and standard deviations are reported for all averages except κ, which is reported as geometric means and standard deviations. All concentrations are reported for ambient conditions.

The CCN behavior showed distinct differences between the different air masses as shown in Fig. 4. The predicted concentrations (assuming pure ammonium sulfate; κ=0.61) are compared to the observed CCN concentrations; the observations are color-coded according to the supersaturation at which CCN was measured, and different shapes indicate the different air mass type. Measurement supersaturations varied with altitude due to the effect of changing inlet pressure (cf. Sect. 2.1.1). The 1:1 line is shown, indicating CCN activity of ammonium sulfate particles. As expected, the predicted concentrations overestimate the CCN concentrations when compared to the ammonium sulfate case for many of the legs, particularly for legs flown in the boundary layer. However, many legs in the free troposphere at low supersaturation appear to have CCN activity greater than that of ammonium sulfate. This result is likely due to the relatively large uncertainties that were associated with the calculation of critical diameters for air masses in the free troposphere (cf. Sect. 4.2). In the following sections, we describe the CCN activity of the different regions in relation to aerosol chemistry and discuss in detail case studies for a few individual flight legs.

Table 3. Summary of measurements and calculated parameters for each air mass category. Values shown are arithmetic mean and standard deviation (in parentheses) of single values obtained for each leg within the designated air mass category unless otherwise indicated. All mass and number concentrations are reported for ambient temperature and pressure.

Air Mass Type	CN cm^{-3}	S_v %	N_{tot} cm^{-3}	$D_{pg}(m^2)^a$ nm	stdev$(m^2)^a$ nm	CN$(m^2)^a$ cm^{-3}	$f_{CCN/CN}$ (ratio)	d_{pc} nm	κ^b –
Free Troposphere (20)	419 (231)	0.20 (0.03)	229 (127)	104 (21)	1.9 (0.19)	322 (117)	0.60 (0.23)	73 (16)	0.98 (2.4)
Marine BL (6)	793 (370)	0.35 (0.01)	156 (85)	136 (23)	1.6 (0.17)	193 (152)	0.26 (0.21)	85 (18)	0.21 (2.0)
Continental BL (7)	18700 (12500)	0.34(0.003)	1560 (900)	97 (23)	1.6 (0.10)	2610 (1410)	0.09 (0.04)	80 (6)	0.25 (1.3)

[a] Geometric median, standard deviation, and CN concentration in "mode 2", the dominant CCN-active mode;
[b] geometric mean and standard deviation.

Table 4. Bulk submicron mass concentrations (µg m^{-3}), non-refractory organic mass fractions (nrOMF), and oxygen-to-carbon ratios (O/C) measured by HR-ToF-AMS for air mass categories. Standard deviations are shown in parentheses. The number of flight legs analyzed for each air mass category is shown in parenthesis in the first column.

Air Mass Type	SO_4	NH_4	NO_3	Organic	nrOMF	O/C
Free Troposphere (20)	0.62 (0.53)	0.15 (0.08)	0.02 (0.02)	0.28 (0.27)	0.17 (0.09)	0.84 (0.23)
Marine BL (6)	0.51 (0.27)	0.11 (0.05)	0.02 (0.01)	0.24 (0.29)	0.18 (0.16)	0.50 (0.22)
Continental BL (7)	1.01 (0.46)	0.42 (0.21)	0.43 (0.41)	2.9 (1.45)	0.50 (0.16)	0.57 (0.02)

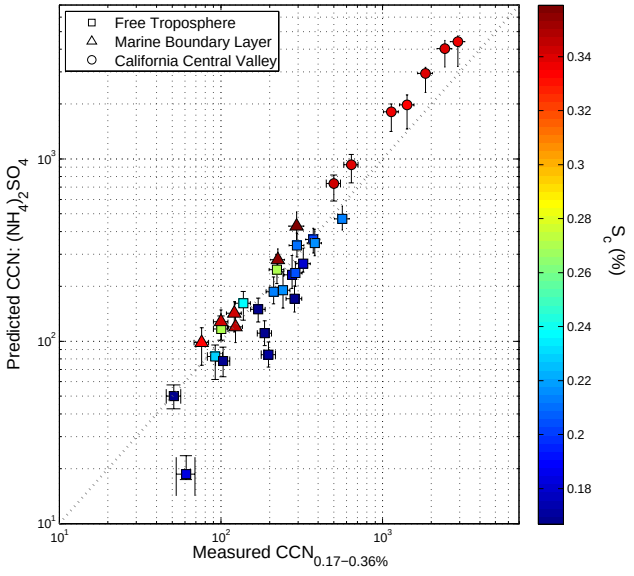

Fig. 4. Predicted CCN vs. measured CCN. Predicted CCN were calculated using pure $(NH_4)_2SO_4$ composition and the Köhler theory. Markers are color-coded for the supersatuation at which the CCN measurements were made. Different air mass regions are indicated by marker shape and a grey line indicates the 1:1 line. Error bars shown for x-axis represent uncertainty in CCN measurements derived from variability during flight leg ($\sigma n^{-0.5}$). Error bars shown for y-axis are derived from variability in SMPS measurements ($\sigma n^{-0.5}$) during each level leg.

3.1 Free troposphere

Flight legs analyzed in the FT were all higher than 2000 m a.s.l. (meters above sea level) and above the Pacific Ocean or inland within 100 kilometers of the coast. As discussed in Sect. 2.1.5, most FT observations showed back trajectories clearly indicating long range transport from Asia. FT observations were characterized by low CN and CCN concentrations ($419\pm231\,cm^{-3}$ and $229\pm127\,cm^{-3}$ ($\sim$0.2% Sc), respectively), and typically a single mode with median diameter 104 ± 21 nm, and showed a wide range of organic ($<$0.1–1 µg/m^3) and sulfate ($<$0.1–2.2 µg/m^3) bulk sub-micrometer concentrations but always with a large inorganic mass fraction (nrIMF; 0.65–0.95). Organic oxygen-to-carbon ratios were the highest of the three air mass types (0.84 ± 0.23). Size distributions (Fig. 5a) showed one dominant broad mode centered at 105 nm suggesting that new particle formation had not recently occurred in these air masses. One FT air mass showed a noticeable smaller mode ($D_p<20$ nm), which was collected at $\sim$500 km off the coast of Alaska and was associated with rapid long range transport from East Asia ($<$3 days); this measurement is omitted from Fig. 5a. Two other measurements (RF4, 5000 m and 5600 m) showed a secondary mode at $\sim$35 nm with similar concentrations to the larger mode (these distributions resulted in the small shoulder shown in Fig. 5a). Similar to the leg showing the $D_p<20$ nm mode, these legs were associated with some of the lowest organic and sulfate concentrations (combined: <0.25 µg/m^3).

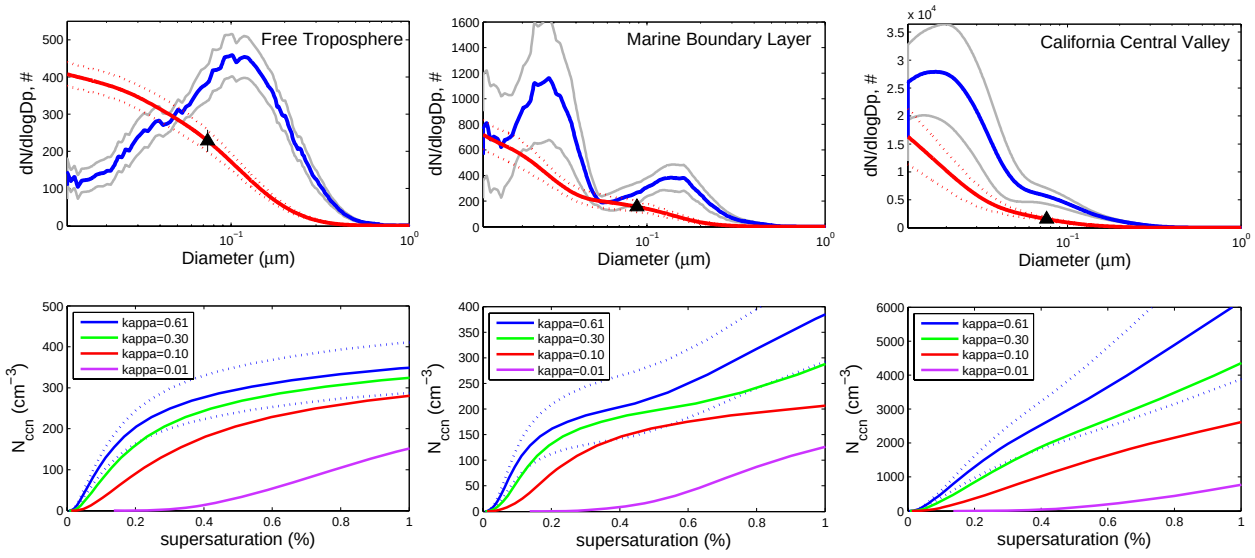

Fig. 5. Average of size distributions and calculated CCN spectra for all level legs in the **(a)** free troposphere, **(b)** marine boundary layer, and **(c)** California Central Valley. Upper panels: blue lines show average size distributions measured by SMPS. Grey lines indicate the 1-sigma standard deviation of the mean of the size distributions for the different level legs ($\sigma n^{-0.5}$). The red lines represent the integrated number concentrations of the size distributions and variation ($\sigma n^{-0.5}$). The average CCN concentrations and variation ($\sigma n^{-0.5}$) are indicated by a black triangle and vertical line. Lower panels: CCN spectra for each air mass using the average size distributions and plotted for aerosol compositions corresponding to four different values for κ. The error in the CCN spectrum attributed to the variance in size distribution is shown for the κ=0.61 (dotted blue lines).

CCN spectra for each level leg were calculated using the average size distributions measured by the SMPS for different chemical component mixtures as described in Sect. 2.1.1. The spectra for the average of all FT legs are shown in Fig. 5a. Variability in the CCN measurement is shown indicating the root mean square ($\sigma n^{-0.5}$) of all level leg averages. The CCN measurements are consistent with the spectra close to the case of a pure ammonium sulfate composition. Using average size distributions and CCN concentrations for each level leg in the FT yield values of 73±16 nm and 0.98 for d_{pc} and κ, respectively (cf. Table 3). The inorganic mass fraction, which is associated with soluble ions, is relatively high at 0.83 (bulk AMS observations) and likely contributes to the high κ values. Moreover, as noted above, the FT organic O/C ratio (as measured by the AMS) was on average 0.84, indicating that organic mass contained in submicron particles in the FT was highly oxidized, suggesting an aged and likely water soluble organic content (Kondo et al., 2007; Jimenez et al., 2009). The two FT legs where back trajectories point to origins in the central Pacific Ocean (2300 m during RF 11 – 11 May) exhibited κ values close to 0.25 (the lower end for κ in FT; with nrOMF<0.10), which may suggest that polluted air masses enhance the rate at which particles become hygroscopic as Asian outflow contains elevated concentrations of sulfate and aerosol precursors (Clarke et al., 2004). It is worth noting that Asian plumes reaching Whistler Peak in Canada (Leiatch et al., 2009) during the INTEX-B study showed a significant reduction of fine particle organic material, as organic compounds preferentially attached to coarse dust particles. As discussed in Roberts et al. (2002) and Sullivan et al. (2009), once particles become sufficiently hygroscopic (κ∼0.25), the critical supersaturations associated with CCN active particles become less sensitive to changes in aerosol chemical composition. The high CCN activity observed in the free troposphere suggests an aging process. Aging within the FT appears to increase CCN-derived hygroscopicity and reduce the heterogeneity (as indicated by the high and similar κ observed in the FT), rendering particles more CCN active regardless of their origin.

Dust from the Gobi and Taklimakan deserts is a known source of dust aerosol in long-range transport across the Pacific Ocean. Aerosol scattering measurements suggested that high dust events accounted for <6% of the INTEX-B flight time (Dunlea et al., 2009). While STXM and XRF provide markers for dust, the AMS cannot detect dust tracers, meriting further discussion here. Some size distribution for FT flight legs did show a mode with much smaller number concentration at ∼600 nm which may be associated to dust or aged aerosol transport (RF9, 8 May 2006). While this large mode contributes negligibly to the overall CCN concentrations at supersaturations greater than 0.1%, it likely contributes to giant CCN and IN. Chemical evidence from single particle analysis further suggests that air masses sampled in the FT may have undergone long-range transport from Asia. Single particle analysis during RF9 (8 May 2006, 5600 m) showed that five of the nine particles analyzed by STXM-

NEXAFS were characterized as combustion-type particles with diameters of 0.4–1 µm. In another flight (RF11, 11 May 2006, 3800 m), 5 of the 10 particles analyzed by STXM-NEXAFS were related to combustion sources (two of the ten particles were characterized as 'Combustion-type' particles, and the other three were type "*k*" – which may also be related to combustion sources as described by Takahama et al., 2007). Our chemical analysis further supports earlier research (Clarke et al., 2001; Hadley et al., 2007) that combustion sources either from anthropogenic emissions in Southeast Asia or biomass burning in Siberia contribute to a significant fraction of long-range transport from Asia. Also, more than a third of the particles collected in the FT over the Pacific that were not identified with combustion were supermicron, evidence that dust may have also been a significant aerosol source (by mass) in air masses sampled. Moreover, the STXM-NEXAFS analysis showed that most of the commonly observed particle spectra types during INTEX-B were also observed during the ACE-ASIA campaign when Asian outflow was sampled over the northwestern Pacific (closer to dust and anthropogenic emissions). The common aerosol types on both sides of the Pacific Ocean suggest that long-range transport is an important particle classification over the Pacific Ocean. During INTEX-B, elevated concentrations of some trace metals associated with anthropogenic sources (Zn, V, Ni, Ba, Si, and Al) were also observed in air masses sampled in the free troposphere (Day et al., 2009), yet another indication of long range transport of anthropogenic and dust particles.

3.2 Marine boundary layer

Several short, low altitude (<500 m a.s.l.) flight legs were conducted within the marine boundary layer (MBL) from 70 to 850 km from the North American coast during INTEX-B. Back trajectories indicate that MBL flight legs did not have recent contact with the North American continent and generally spent the previous week in the North Pacific, and therefore were likely not affected by anthropogenic sources in the 24 h prior. Also, trace gases associated with continental influence (CO, NO_y, NO_x) were always observed at background concentrations (142–147 ppb, 0.2–0.3 ppb, 25–50 ppt, respectively). Marine boundary layer observations showed similar CN concentrations to the FT (793±370 cm^{-3}). However, two modes were often observed with a larger mode diameter at 136±23 nm with a majority of total particles in a smaller, non CCN-active mode with D_p∼30 nm (with the exception of one leg during RF 11; Lat: 44.11, Lon: −125.23, Alt; 170 m). Figure 5 shows the average distribution for all MBL flight legs. The large ultrafine mode in the size distributions may result from entrainment from above (Russell et al., 1998), shipping emissions, or a marine source (Clarke et al., 1998). CCN concentrations were lower than both other air mass types (∼0.35% Sc; 156±85 cm^{-3}). Sulfate and organic mass were generally low and similar to the FT (averages: 0.51; 0.24 µg/m^3, respectively) and the nrOMF was variable (0.03–0.44). Sulfate and nrOM ranged from 0.3 to 1.0 µg/m^3 and <0.1 to 0.8 µg/m^3, respectively. On average, organic O/C ratios were lower for the MBL air masses (0.50±0.22) than the FT and CCV air mass types, suggesting that the organic mass present in the MBL is not highly oxidized, and possibly less soluble than for the other air masses.

In these six legs in the MBL, two during RF02, two during RF05, and one during RF9 and RF11; Table 1), the CCN measurements had an average κ of 0.21 (at ∼0.35% Sc) with an average d_{pc} of 85±18 nm. The right panel of Fig. 5b shows the CCN spectra calculated using the average size distributions for particles with a range of κ values for reference. The spectra calculated using the AMS bulk concentrations (not shown) was similar to the κ=0.61 spectrum, indicating that the bulk concentrations significantly over predicted CCN activity. For nrOM concentrations <0.5 µg/m^3 and for typical level leg duration (∼10 min), it was not possible to obtain size distributions of nrOM with the AMS.

In some MBL samples nrOM O/C ratios were low, suggesting either primary marine emissions or recently formed SOA. It is possible that the aerosol in these air masses are externally mixed, with smaller organic-rich or soot particles with low CCN activity, that exert a significant effect on the average κ calculated. No samples were available for single particle analyses by STXM for the six flight legs identified as entirely in the MBL. However, particles were analyzed for one flight leg that occurred at the interface between FT and MBL (∼850 m a.s.l.). Potential temperature and relative humidity observations suggest that this leg may have partly consisted of MBL sampling. In addition, back trajectories for 500, 850, and 1200 m indicated that this air mass did not pass over land in the prior 7 days. The 27 particles analyzed with STXM for this leg showed a variety of particle types (7 secondary, 5 combustion, 5 Ultisol, and 4 Biomass) suggesting possible combustion origins and aging processes above the Pacific Ocean. Of the 27 particles collected during this leg and analyzed with STXM, only two supermicron particles showed cuboid morphology typically associated with salt particles. Moreover, of the four FTIR spectra associated with MBL sampling, none showed evidence of an organic marine signature associated with absorption in the alcohol region of the spectra (Russell et al., 2010), and submicron Na (XRF) was always below detection limit. These results suggest that shipping-related pollution could be an important contribution to particle mass in otherwise pristine maritime atmosphere.

The presence of an ultrafine mode in the MBL could also be the result of entrainment from the clean FT (e.g. Clarke and Kapustin, 2002). There were no level legs flown just above the MBL in the vicinity of MBL air masses analyzed here, so a complete CCN analysis of these altitudes was not possible.

3.3 Continental boundary layer

While not the focus of the INTEX-B experiments, several low altitude (∼500 m a.s.l.) flight legs were conducted in the California Central Valley (CCV) within the continental boundary layer. We analyzed all CCV sampling legs where relevant measurements were available (7 legs). Total CN concentrations were high (5000–25 000 cm^{-3}), with the majority <50 nm diameter, indicative of nearby sources of new particle formation and emissions in this heavily urban influenced region. Figure 5c shows the average and variability of the CCV size distributions. CCN concentrations were also much higher than the other air mass types, averaging 1560±900 cm^{-3} at ∼0.35% Sc. nrOM and sulfate were variable among legs with concentrations of 2.9±1.5 µg/m^3 and 1.01±0.46 µg/m^3, respectively, while the nrOMF showed much less variability (0.50±0.16). CCN observations (at ∼0.35% Sc) yielded κ values of 0.25 with an average d_{pc} of 80±6 nm. Despite the much higher particle concentration and proximity to anthropogenic sources in the polluted continental boundary layer, average κ were similar to, yet less variable than for the MBL (0.21±2.0).

Figure 5 shows CCN spectra for the average of all CCV flight legs. The AMS size distributions from the CCV had sufficient signal-to-noise to show that the submicron particles showed evidence of external mixing with a sulfate mass mode centered at ∼350 nm and the nrOM mode centered at ∼200 nm. The results suggest that particles with sizes near the critical diameter were comprised mostly of nrOM volume fraction.

Measurements with AMS (cf. Table 4) and FTIR (Day et al., 2009) showed that CCV had higher submicron nrOM concentration than the free troposphere and marine boundary layer air masses and significantly lower O/C ratios than the free troposphere, both factors that may account for the lower κ found in the CCV than in the FT. No STXM analysis was performed for CCV flight legs since the FT was targeted as the primary focus region during this campaign. While the AMS bulk concentrations (not shown) yielded κ values similar to those observed, we note that most of the mass detected by the AMS is for particles larger than those that contribute the majority of the CCN number. Since the AMS measures the inorganic ions that strongly influence CCN activity (i.e., sulfate and nitrate), the apparent agreement between bulk measurements and observed κ values may be due to compensating errors rather than a confirmation of the usefulness of using bulk measurements to predict CCN concentrations.

4 Discussion

4.1 Observed hygroscopicity parameters

Significant differences in κ were observed between the free troposphere and boundary layer air masses. Few observations of κ for the free troposphere have been reported. Average κ values for the three major air mass classifications are shown in Table 3. The κ values in the marine boundary layer and California Central Valley were similar (0.25 and 0.21 at ∼0.35% Sc, respectively), while κ values in the free troposphere were considerably higher (0.98 at ∼0.2% Sc). Figure 6 (middle panel) shows the relationship between H-TDMA and CCN derived κ (κ_{H-TDMA} and κ_{CCN}) to nrOMF and clearly shows separation based on air mass category. The trend shows an increase in κ with decreasing nrOMF, which has been reported in Shinozuka et al. (2009) for the INTEX-B experiment as well as in the Amazon (Gunthe et al., 2009). The Shinozuka et al. Fig. 2a κ values derived from the CCN measurements correspond to airmasses >3000 m above the Pacific Ocean or the North American continent (2009); however here we have extended the analysis to include MBL an CCV air masses. Particle hygroscopicity was analyzed for similar air mass categories during the Cloud Indirect Forcing Experiment (CIFEX; Roberts et al., 2006), which also studied long-range transport into Northern California during Spring 2004. The κ observed during CIFEX (derived from a single particle parameter presented as an "activation index") are shown in Table 5 for comparison to INTEX-B observations. CCN measurements during CIFEX were performed with the University of Wyoming static CCN chamber at 0.2% and 0.4% Sc). The κ values from the MBL and North American air masses during CIFEX are lower than those values reported during the INTEX-B experiment (0.05 compared to 0.2, respectively). The largest κ observed during CIFEX (κ=0.61) were associated with cloud processed particles at 0.2% Sc. Hygroscopicity parameters were not determined in the free troposphere during CIFEX; however, Wang et al. (2008) report κ in the free troposphere using CCN and AMS observations as κ∼0.38 (based on particles with 43% ammonium bisulfate, 7% nitrate, and 50% organic by volume). Values for κ observed in the FT during INTEX-B were consistently at the upper range of the other limited FT measurements with almost no overlap with κ for the other air masses sampled during this study.

The marine boundary layer κ values for CIFEX and INTEX-B are lower than MBL measurements by Hudson (2007) and Shantz et al. (2008). Hudson (2007) report

Table 5. κ values for different air masses during the CIFEX experiment (Roberts et al., 2006).

	CIFEX κ (0.2% Sc)	CIFEX κ (0.4% Sc)	INTEX-B
Marine	–	0.06	0.21 (∼0.3% Sc)
North American/urban	0.05 (0.03–0.09)	0.04	0.25 (∼0.3% Sc)
Aged aerosol layers	0.04	0.02	–
Cloud-processed	0.61	0.13	–
Free Troposphere	–	–	0.98 (∼0.2% Sc)

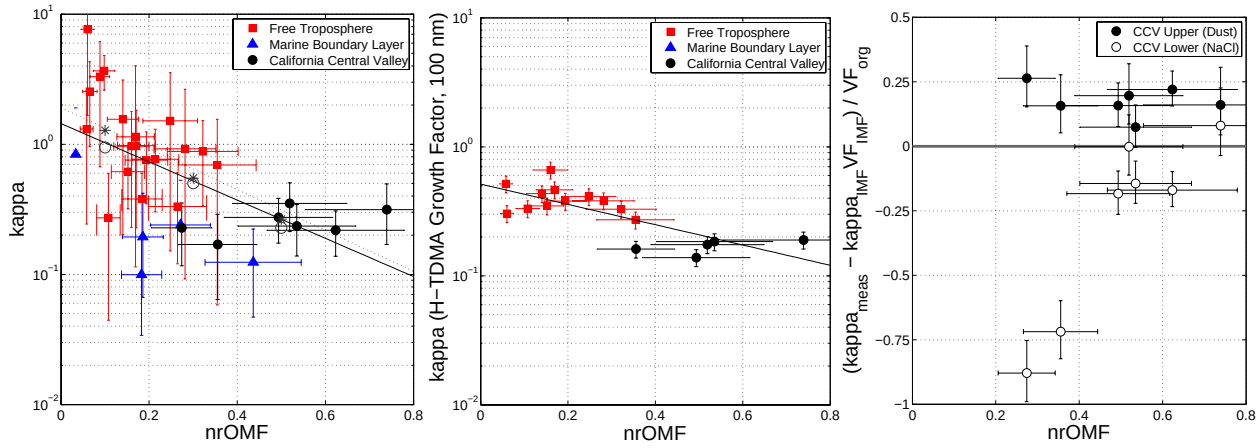

Fig. 6. κ vs. non-refractory organic mass fraction (nrOMF). The left panel shows κ values calculated using CCN and size distribution measurements. Error bars for κ were calculated by computing the certainty in the calculated dry critical diameter (d_{pc}) using the variability in the SMPS size distributions and CCN measurements ($\sigma n^{-0.5}$) for each flight leg; the uncertainty d_{pc} was propagated with the supersaturation error (20%) to yield the κ error. Error bars for the nrOMF were calculated from the variability in the AMS nrOM during the flight leg ($\sigma n^{-0.5}$), combined in quadrature with a 20% uncertainty typically associated with AMS nrOM measurements and 15% associated with aerosol volume (SMPS). The lines indicate the best fit line to all data (black) and omitting MBL data (grey). Grey circles (all data) and grey asterisks (omitting MBL) are binned averages for nrOMF ranges 0–0.2, 0.2–0.4, and 0.4–0.6. The middle panel shows κ values calculated using H-TDMA growth factor measurements for particles of size 100 nm (error: ±15%). The right panel shows the difference of measured κ and the κ calculated using inorganic components only (normalized to the organic volume fraction, VF_{org}), an estimate of κ_{org} (see text for details). Y-axis error bars shown here are κ_{meas}/VF_{org}.
Line Fits for left panel:
all data fit (dark line): $r = -0.57$; $\log(\kappa) = -1.5(\text{nrOMF})+0.2$
Excluding MBL (light line): $r = -0.67$; $\log(\kappa) = -1.6(\text{nrOMF})+0.3$.
Line Fit for middle panel:
$r = -0.77$; $\log(\kappa) = -0.79(\text{nrOMF})-0.29$.

κ=0.31 to 0.34 at 100 m below the stratocumulus cloud deck and κ=0.11 above cloud deck off the central California coast during the Monterey Area Ship Tracks Experiment (MAST). In an experiment at a pristine Caribbean site, they report κ=0.59 to 1.11 in the MBL. Shantz et al. (2008) present a case study using size-resolved aerosol composition (AMS and MOUDI), CCN concentration, and size distribution measurements conducted from a ship platform in the Northeastern Pacific. They calculate an average κ value of 0.35 for a period with elevated organics ($\sim$1 µg m^{-3}), with H_2SO_4 constituting the remainder of the submicron aerosol mass ($\sim$1.5 µg m^{-3}). Similarly, CCN measurements during an airborne experiment studying marine stratocumulus clouds off the coast of California observed κ=0.35 in the lower MBL with a nrOMF fraction approximately 50% (Wang et al., 2008). In air masses just above the marine cloud layer, Wang et al. (2008) determined κ=0.15 largely due to the $\sim$90–95% nrOM as observed in the size-resolved AMS measurements. Their study shows that the non-zero κ($\sim$0.1) of the organic fraction becomes important as the water-soluble inorganic fraction tends to zero – which is dictated by the sensitivity of CCN activation to a small amount of water-soluble species (Roberts et al., 2002). These results show that values for hygroscopicity parameters can vary between less hygroscopic (κ<0.1) to very hygroscopic (κ=0.6) in the MBL, with a general reported value near 0.3.

Several studies have shown that a substantial fraction of marine particles is composed of organic compounds (e.g. Novakov et al., 1997; Middlebrook et al., 1998; Wang et al., 2008). In some cases, the impact of organic compounds on kappa in MBL aerosols can be profound (Wang et al., 2008; where the organic fraction approaches 95%). In other cases, the impact is likely less significant (Phinney et al., 2006; where the organic fraction is less than 25%). Russell et al. (2010) observed that the organic component constituted large parts of the submicron mass and suggest the primary source of the organic aerosol component is emitted through bubble-bursting processes within the ocean surface microlayer. Their results point to a large organic contribution that may be non-hygroscopic. Furthermore, recent field studies (Modinia et al., 2010) suggest that organic films on marine particle may significantly suppress the water uptake of mixed particles in H-TDMA measurements.

Similar to results in an urban, polluted environment observed during INTEX-B, Rose et al. (2010) report an average κ value of $\sim$0.3 for highly polluted air; CCN concentrations in a mega-city in China averaged 6500 cm^{-3} (at S_c=0.27%). CCN concentrations in the CCV during INTEX-B averaged

2600 cm^{-3} with κ=0.25 (S_c=0.34%; Table 5). The hygroscopicity parameter for North American aerosols in CIFEX is considerably lower; however, airborne measurements of aerosol composition were not collected during CIFEX and cannot be related to observations of κ. In a review of H-TDMA observations, Swietlicki et al. (2008) also report a large range of growth factors observed in the urban environment; however, the timescales of aging processes that render the aerosol more hygroscopic are not well understood. CCV air masses sampled here were from a limited geographic region and showed relatively similar chemical compositions; however, they provided a large contrast in both hygroscopicity and chemical composition compared to the FT air masses.

4.2 H-TDMA and CCN hygroscopicity parameters

The coincident measurements of the hygroscopic growth factors using a H-TDMA provided a valuable opportunity to compare the two principal field methods in use for investigating aerosol hygroscopicity under a wide range of sampling conditions. Although both techniques probe aerosol hygroscopicity, the H-TDMA method typically targets discrete aerosol sizes, whereas coupling of CCN and SMPS measurements provides information for the ensemble of particles larger than the critical diameter for the measured supersaturation. During INTEX-B, hygroscopic growth factor measurements using a H-TDMA (RH 85%) typically showed large decreases from ca. 1.5 in the continental free troposphere to ca. 1.15 in the CCV for particle sizes 25, 50, and 100 nm (but generally not for 300 nm). This trend is consistent with our observations of κ between FT and MBL or CCV. The average κ in the CCV calculated from the H-TDMA for 100 nm particles ($\kappa_{\mathrm{H-TDMA}}$=0.17) were approximately half those calculated for the FT legs ($\kappa_{\mathrm{H-TDMA}}$=0.39). A similar comparison was not possible for the MBL since these legs were too short (~5 min) and few growth factor measurements were recorded during these legs. Figure 7 shows a comparison of the κ_{CCN} and $\kappa_{\mathrm{H-TDMA}}$ (from TAMU H-TDMA growth factor measurements). A common trend between FT and CCV hygroscopicity parameters is observed in Fig. 7, while the ratio of $\kappa_{\mathrm{H-TDMA}}$ to κ_{CCN} averages 0.43. Brechtel and Kreidenweis (2000) report discrepancies of up to 65% between H-TDMA supersaturations and measurements with a CCN instrument for ambient particles. Yet, Vestin et al. (2007) show reasonable agreement between observed CCN concentrations and predictions based on H-TDMA growth factor measurements (and H-TDMA single parameter approximation). Swietlicki et al. (2008) note that the relative humidity in H-TDMA measurements should be at least 90% to improve accuracy of growth factor measurements when extrapolating to supersaturations in CCN instruments. However, large uncertainties were apparent in κ derived from coupling the independent CCN and size distribution measurements, as evident in the large error bars and κ values that are not physically realistic (κ>1). Relative errors for the FT tended to be

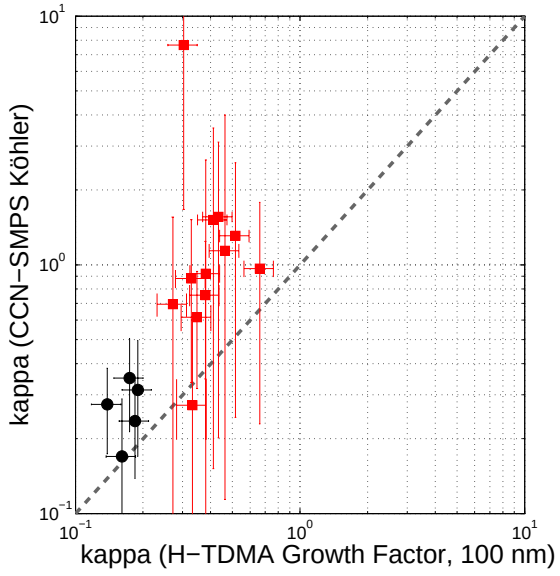

Fig. 7. κ is calculated with CCN-SMPS (Köhler) and H-TDMA particle growth factors. Line shown is 1:1. See Fig. 6 caption for error bars.

large, in part due to the flat slope of the cumulative CN distribution for a range of sizes surrounding the critical diameter. This flat feature can lead to large changes in the calculated critical diameter with small changes in CCN or size distribution concentrations, even though it is not evident in the average of cumulative CN distributions shown in Fig. 5a). Therefore, the overall chemical and geographic trends of κ are the most important results of this study.

4.3 Relating κ to organic composition

The trend between κ and nrOMF in Fig. 6 (left panel) has been proposed as a simple linear combination of the contribution of water-soluble salts and less water-soluble organic fractions to overall water activity (Gunthe et al., 2009). Similarly, a linear parameterization has been described for the relationship between aerosol light scattering and [nrOM]/[nrOM+SO_4] which results from an increase in hygroscopicity with decreasing organic fraction and thus greater water uptake and particle growth (Quinn et al., 2005). However, there is increasing evidence that the chemical composition of the organic component can exert important controls over aerosol hygroscopicity and may be related to source types, aging processes, or SOA formation (e.g. Clarke et al., 2007; Chang et al., 2010; Jimenez et al., 2009; Raatikainen et al., 2010). In order to assess potential effects of the organic component on CCN activity we compare the measured κ values to κ values calculated using only the inorganic components (κ_{IMF}). As Petters and Kreidenweis (2007) show, the overall κ can be approximated as the sum of the volume-weighted κ for each separate chemical

component. κ_{IMF} was calculated for each flight leg using average bulk concentrations of NR compounds (AMS) plus BC with the aerosol volume that was not chemically resolved and assumed to be refractory (not BC) calculated with the additional information provided by the SMPS submicron size distributions. The non-BC refractory (nBC-R) volume was calculated as the difference between the cumulative volume for submicron aerosol SMPS measurements and the volume derived from the NR and BC concentrations (and assumed densities: Table 2). Ratios of NR+BC to SMPS volume was on average 0.74±0.32.

The ammonium was associated with sulfate and nitrate as described in Sect. 2.2.1 and limiting cases were calculated by assigning the nBC-R to either dust ($\kappa \sim 0$) or NaCl (κ=1.28). Values used for individual κ were: 0.61 (AS), 0.7 (ABS), 0.90 (SA), 0.67 (AN), and 0 (BC) (values from Petters and Kreidenweis (2007) with ABS approximated as slightly more hygroscopic than a AS-ABS binary mixture (0.65)). This treatment showed that the measured particles were nearly always a mixture of AS-ABS and rarely that of SA-ABS (never in the FT). This result, in combination with the likelihood that at the nominal 30% RH of the aerosol measurements, means that assigning the exact AS-ABS-SA composition is probably not critical. Moreover, these factors suggest that high SA or ABS fractions are not likely to be the cause of $\kappa > 0.7$ in the FT.

The results are shown in Fig. 6 (right panel) plotted vs. nrOMF. The values associated with the y-axis represent an estimate for the κ related to organics (κ_{org}). Only results for the CCV air masses are shown. Uncertainties associated with the measured FT κ were too large to determine κ_{org} for the FT air masses with adequate confidence, resulting in scattered values that are indistinguishable from zero. The larger uncertainties are expected for the FT, since their small nrOMF contributes little to reducing the overall κ. For the MBL air masses κ_{org} was always negative, suggesting an overestimate in the inorganic hygroscopicity contribution derived from the bulk chemical inorganic components. For the CCV air masses, the dust-limit case (more realistic for the CCV) shows an average κ_{org} of 0.18±0.06, which corresponds to the lower limits for CCN and H-TDMA derived k. This is a realistic value to which we assign moderate confidence.

In order to investigate the effects of organic composition on the hygroscopicity a similar plot can be constructed, comparing the estimated κ_{org} to the nrOM O/C ratio (Fig. 8). Also shown on the plot (green line) is the approximate relationship shown for κ_{org} vs. O/C reported by Jimenez et al. (2009) (κ_{org}=0.49·(O/C−0.25) for O/C≥0.25, and κ_{org}=0 otherwise), with the solid line covering the range of their data, and the dotted line extrapolated to O/C=1.2. The κ_{org} calculated for the CCV (dust-limit) is in acceptable agreement with the relationship described in Jimenez et al. (2009) (i.e., 0.18±0.06 compared to 0.15 from fit), providing evidence that nrOM O/C can be used to predict κ_{org}. However,

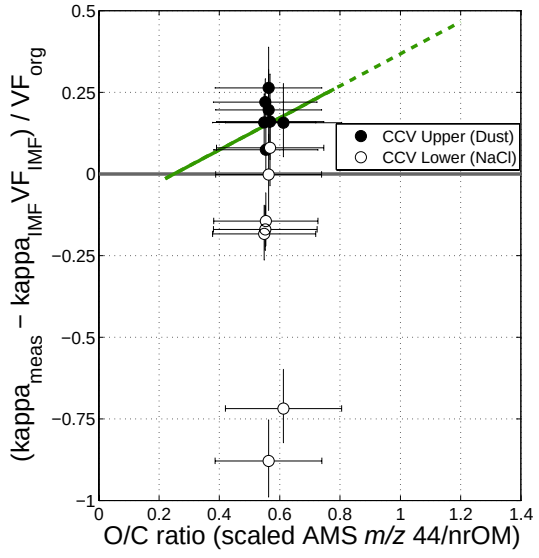

Fig. 8. Estimated κ_{org} vs. O/C ratio. Solid symbols represent the limit in which the mass not chemically resolved by AMS+BC (compared to that estimated from size SMPS distributions) is approximated as dust. Open symbols represent the case where the chemically un-resolved mass is approximated as NaCl. See Fig. 6 for κ_{meas} error description. Y-axis error bars shown here are κ_{meas}/VF_{org}. The error bars shown for the O/C ratio were calculated from the variability in the AMS nrOM and *m/z* 44 measurements ($\sigma n^{-0.5}$ for each and sum of squares of relative errors) and combined with a ∼35% uncertainty associated with derived O/C ratios with this method (Aiken et al., 2008).

a wider range of O/C and air mass regions with more precise determinations of κ_{org} would be required to bolster the case for the apparent agreement. Since the errors in these values are the same as those in Fig. 6, and therefore the uncertainties are too large to evaluate the effect of O/C on κ_{org} for the FT and MBL samples.

We did not observe any identifiable trend in FT κ with longitude, suggesting that significant changes in hygroscopicity do not occur in the eastern Pacific in air transported from Asia. The similarity of the carboxylic carbonyl carbon-to-total carbon ratios for the smallest particles collected and analyzed with STXM-NEXAFS during this study to those observed by Maria et al. (2003) also suggested that on average particles transported from Asia may undergo most of the oxidation over the western Pacific (Day et al., 2009). Similar to κ, the carboxylic carbonyl carbon-to-total carbon ratios did not show any longitudinal trends in the samples collected in the eastern Pacific. However, Dunlea et al. (2009) report evidence that plumes transported more slowly from Asia to the Eastern Pacific showed a greater degree of oxidation of organic aerosol.

5 Conclusions

These measurements provide the first application of the DMT-CCN instrument for a full range of different ambient pressures as part of aircraft measurements during level legs, as well as a detailed characterization of the temperature gradient and pressure dependence in the laboratory. A wide range of air masses was sampled that showed distinct differences in hygroscopicity and chemical composition. The three types of air masses sampled included FT and MBL particles with large nrIMF and CCV particles with large nrOMF. CCN concentrations were much larger for the polluted CCV compared to the MBL, however they showed similar κ values (0.2–0.25). CCN concentrations were lowest in the free troposphere and κ was consistently higher than for other air masses, consistent with the associated high inorganic mass fractions. The analysis of CCN activity in the free troposphere presented here adds to an extremely sparse number of studies of CCN anywhere within the free troposphere.

For the CCV, calculations of κ using bulk submicron chemical composition measurements (AMS) predicted κ values that were similar to κ derived from CCN and size distribution measurements. In contrast, use of bulk chemical measurements consistently over-predicted CCN activity for the marine boundary layer, likely due to external mixtures of particles of different compositions or to particle mass being dominated by particle sizes larger than many CCN, highlighting the importance of size-resolved and single-particle chemical measurements for investigating CCN activity. All but one of the marine boundary layer air masses displayed a large ultrafine particle mode despite the fact that back trajectories indicated that recent continental influence was unlikely. These results in combination with the large range of κ observed for the marine boundary layer suggests that CCN activity in the MBL is not well understood, possibly due to the presence of a range of sources such as marine emissions, shipping emissions, long-range transported particles, or particle entrainment from the free troposphere.

An overall trend of decreasing CCN activity with increasing bulk organic mass fractions was observed for the free troposphere and CCV air masses. This trend was driven primarily by the inorganic mass fraction rather than changes in the composition of the organic fraction. In the CCV, the normalized organic contribution to κ, i.e. κ_{org}, was 0.18 ± 0.06, which is consistent with laboratory and other polluted atmospheric particles. Given the range and uncertainty of the observed κ, correlations between either the O/C ratio and the organic contribution to κ were not observed. No trends were observed with longitude, suggesting that major processes that effect κ occur within a few days of trans-Pacific long-range transport.

Comparison of CCN-derived κ (at critical diameter) to H-TDMA-derived κ (at 100 nm diameter) showed similar trends, however the CCN-derived κ were significantly higher. As highlighted by recent measurements of CCN and aerosol size distributions (Good et al., 2010 and Duplissy et al., 2009), thediscrepancy H-TDMA and CCN-derived kappaswarrants further investigation, particularly under the challenging conditions present in aircraft platform sampling.

Acknowledgements. Grant support for this work was provided by NSF (ATM 05-11772). In addition we are grateful to Greg Kok, Stefania Gilardoni, and the NCAR C130 crew for valuable assistance during sample collection. We also acknowledge Laurent Gomes, Brigitte Gaillard and Thierry Bourrianne at CNRM-Météo France (Toulouse) for their assistance with the calibrating the CCN instrument.

Edited by: H. Singh

References

Aiken, A. C., DeCarlo, P. F., and Jimenez, J. L.: Elemental analysis of organic species with electron ionization high-resolution mass spectrometry, Anal. Chem., 79, 8350–8358, doi:10.1021/ac071150w, 2007.

Aiken, A. C., Decarlo, P. F., Kroll, J. H., et al.: O/C and OM/OC ratios of primary, secondary, and ambient organic aerosols with high-resolution time-of-flight aerosol mass spectrometry, Environ. Sci. Technol., 42, 4478–4485, doi:10.1021/es703009q, 2008.

Andreae, M. O.: A new look at aging aerosols, Science, 326, 1493–1494, doi:10.1126/science.1183158, 2009.

Bigg, E. K.: Technique for studying the chemistry of cloud condensation nuclei, Atmos. Res., 20, 75–80, 1986.

Bond, T. C. and Bergstrom, R. W.: Light absorption by carbonaceous particles: An investigative review, Aerosol Sci. Technol., 40, 27–67, doi:10.1080/02786820500421521, 2006.

Brechtel, F. J. and Kreidenweis, S. M.: Predicting particle critical supersaturation from hygroscopic growth measurements in the humidified TDMA. Part II: Laboratory and ambient studies, J. Atmos. Sci., 57, 1872–1887, 2000.

Chang, R. Y.-W., Slowik, J. G., Shantz, N. C., Vlasenko, A., Liggio, J., Sjostedt, S. J., Leaitch, W. R., and Abbatt, J. P. D.: The hygroscopicity parameter (κ) of ambient organic aerosol at a field site subject to biogenic and anthropogenic influences: relationship to degree of aerosol oxidation, Atmos. Chem. Phys., 10, 5047–5064, doi:10.5194/acp-10-5047-2010, 2010.

Chang, R. Y. W., Liu, P. S. K., Leaitch, W. R., et al.: Comparison between measured and predicted CCN concentrations at Egbert, Ontario: Focus on the organic aerosol fraction at a semi-rural site, Atmos. Environ., 41, 8172–8182, doi:10.1016/j.atmosenv.2007.06.039, 2007.

Clarke, A., McNaughton, C., Kapustin, V., et al.: Biomass burning and pollution aerosol over North America: Organic components and their influence on spectral optical properties and humidification response, J. Geophys. Res.-Atmos., 112, D12S18, doi:10.1029/2006jd007777, 2007.

Clarke, A. D., Varner, J. L., Eisele, F., et al.: Particle production in the remote marine atmosphere: Cloud outflow and subsidence during ACE 1, J. Geophys. Res.-Atmos., 103, 16397–16409, 1998.

Clarke, A. D., Collins, W. G., Rasch, P. J., et al.: Dust and pollution transport on global scales: Aerosol measurements and model predictions, J. Geophys. Res.-Atmos., 106, 32555–32569, 2001.

Clarke, A. D., Kapustin, V. N., Shinozuka, Y., Howell, S., Huebert, B., Masonis, S., Anderson, T., Covert, D., Weber, R., Anderson, J., Zin, H., Moore II, K. G., and McNaughton, C.: Size-Distributions and Mixtures of Black Carbon and Dust Aerosol in Asian Outflow: Physio-chemistry, Optical Properties, J Geophys. Res.-Atmos., 109, D15S09, doi:10.1029/2003JD004378, 2004.

Clarke, A. D. and Kapustin, V. N.: A pacific aerosol survey. Part I: A decade of data on particle production, transport, evolution, and mixing in the troposphere, J. Atmos. Sci., 59, 363–382, 2002.

Cooper, O. R., Parrish, D. D., Stohl, A., et al.: Increasing spring time ozone mixing ratios in the free troposphere over the western North America, Nature, 463, 344–348, 2010.

Day, D. A., Takahama, S., Gilardoni, S., and Russell, L. M.: Organic composition of single and submicron particles in different regions of western North America and the eastern Pacific during INTEX-B 2006, Atmos. Chem. Phys., 9, 5433–5446, doi:10.5194/acp-9-5433-2009, 2009.

DeCarlo, P. F., Kimmel, J. R., Trimborn, A., et al.: Field-deployable, High-Resolution, Time-of-Flight Aerosol Mass Spectrometer, Anal. Chem., 78, 8281–8289, 2006.

DeCarlo, P. F., Dunlea, E. J., Kimmel, J. R., Aiken, A. C., Sueper, D., Crounse, J., Wennberg, P. O., Emmons, L., Shinozuka, Y., Clarke, A., Zhou, J., Tomlinson, J., Collins, D. R., Knapp, D., Weinheimer, A. J., Montzka, D. D., Campos, T., and Jimenez, J. L.: Fast airborne aerosol size and chemistry measurements above Mexico City and Central Mexico during the MILAGRO campaign, Atmos. Chem. Phys., 8, 4027–4048, doi:10.5194/acp-8-4027-2008, 2008.

Drewnick, F., Hings, S. S., Alfarra, M. R., Prevot, A. S. H., and Borrmann, S.: Aerosol quantification with the Aerodyne Aerosol Mass Spectrometer: detection limits and ionizer background effects, Atmos. Meas. Tech., 2, 33–46, doi:10.5194/amt-2-33-2009, 2009.

Dunlea, E. J., DeCarlo, P. F., Aiken, A. C., Kimmel, J. R., Peltier, R. E., Weber, R. J., Tomlinson, J., Collins, D. R., Shinozuka, Y., McNaughton, C. S., Howell, S. G., Clarke, A. D., Emmons, L. K., Apel, E. C., Pfister, G. G., van Donkelaar, A., Martin, R. V., Millet, D. B., Heald, C. L., and Jimenez, J. L.: Evolution of Asian aerosols during transpacific transport in INTEX-B, Atmos. Chem. Phys., 9, 7257–7287, doi:10.5194/acp-9-7257-2009, 2009.

Duplissy, J., Gysel, M., Sjogren, S., Meyer, N., Good, N., Kammermann, L., Michaud, V., Weigel, R., Martins dos Santos, S., Gruening, C., Villani, P., Laj, P., Sellegri, K., Metzger, A., McFiggans, G. B., Wehrle, G., Richter, R., Dommen, J., Ristovski, Z., Baltensperger, U., and Weingartner, E.: Intercomparison study of six HTDMAs: results and recommendations, Atmos. Meas. Tech., 2, 363–378, doi:10.5194/amt-2-363-2009, 2009.

Gasparini, R., Li, R., and Collins, D. R., Integration of size distributions and size-resolved hygroscopicity measured during the Houston Supersite for compositional categorization of the aerosol, Atmos. Environ., 38(20), 3285–3303, 2004.

Good, N., Topping, D. O., Allan, J. D., Flynn, M., Fuentes, E., Irwin, M., Williams, P. I., Coe, H., and McFiggans, G.: Consistency between parameterisations of aerosol hygroscopicity and CCN activity during the RHaMBLe discovery cruise, Atmos. Chem. Phys., 10, 3189–3203, doi:10.5194/acp-10-3189-2010, 2010.

Gunthe, S. S., King, S. M., Rose, D., Chen, Q., Roldin, P., Farmer, D. K., Jimenez, J. L., Artaxo, P., Andreae, M. O., Martin, S. T., and Pöschl, U.: Cloud condensation nuclei in pristine tropical rainforest air of Amazonia: size-resolved measurements and modeling of atmospheric aerosol composition and CCN activity, Atmos. Chem. Phys., 9, 7551–7575, doi:10.5194/acp-9-7551-2009, 2009.

Hadley, O. L., Ramanathan, V., Carmichael, G. R., et al.: Trans-Pacific transport of black carbon and fine aerosols (D < 2.5 mu m) into North America, J. Geophys. Res.-Atmos., 112, D05309, doi:10.1029/2006jd007632, 2007.

Hallquist, M., Wenger, J. C., Baltensperger, U., Rudich, Y., Simpson, D., Claeys, M., Dommen, J., Donahue, N. M., George, C., Goldstein, A. H., Hamilton, J. F., Herrmann, H., Hoffmann, T., Iinuma, Y., Jang, M., Jenkin, M. E., Jimenez, J. L., Kiendler-Scharr, A., Maenhaut, W., McFiggans, G., Mentel, Th. F., Monod, A., Prévôt, A. S. H., Seinfeld, J. H., Surratt, J. D., Szmigielski, R., and Wildt, J.: The formation, properties and impact of secondary organic aerosol: current and emerging issues, Atmos. Chem. Phys., 9, 5155–5236, doi:10.5194/acp-9-5155-2009, 2009.

Heald, C. L., Kroll, J. H., Jimenez, J. L., et al.: A simplified description of organic aerosol composition and implications for atmospheric aging., Geophys. Res. Lett., 37, L08803, doi:10.1029/2010GL042737, 2010.

Hudson, J. G.: Variability of the relationship between particle size and cloud-nucleating ability, Geophys. Res. Lett., 34, L08801, doi:10.1029/2006gl028850, 2007.

Jimenez, J. L., Jayne, J. T., Shi, Q., et al.: Ambient aerosol sampling using the Aerodyne Aerosol Mass Spectrometer, J. Geophys. Res., 108(D7), 8425, doi:10.1029/2001JD001213, 2003.

Jimenez, J. L., Canagaratna, M. R., Donahue, N. M., et al.: Evolution of organic aerosols in the atmosphere, Science, 326, 1525–1529, doi:10.1126/science.1180353, 2009.

Köhler, H.: The nucleus in and the growth of hygroscopic droplets, Trans. Farad. Soc., 32, 1152–1161, 1936.

Kondo, Y., Miyazaki, Y., Takegawa, N., et al.: Oxygenated and water-soluble organic aerosols in Tokyo, J. Geophys. Res.-Atmos., 112, D01203, doi:10.1029/2006jd007056, 2007.

Lance, S., Medina, J., Smith, J. N., et al.: Mapping the operation of the DMT Continuous Flow CCN counter, Aerosol Sci. Technol., 40, 242–254, doi:10.1080/02786820500543290, 2006.

Leaitch, W. R., Macdonald, A. M., Anlauf, K. G., Liu, P. S. K., Toom-Sauntry, D., Li, S.-M., Liggio, J., Hayden, K., Wasey, M. A., Russell, L. M., Takahama, S., Liu, S., van Donkelaar, A., Duck, T., Martin, R. V., Zhang, Q., Sun, Y., McKendry, I., Shantz, N. C., and Cubison, M.: Evidence for Asian dust effects from aerosol plume measurements during INTEX-B 2006 near Whistler, BC, Atmos. Chem. Phys., 9, 3523–3546, doi:10.5194/acp-9-3523-2009, 2009.

Lide, D.: Handbook of Chemistry and Physics, CRC Press, Boca Raton, FL, 2010.

Maria, S. F., Russell, L. M., Turpin, B. J., et al.: Source signatures of carbon monoxide and organic functional groups in Asian Pacific Regional Aerosol Characterization Experiment (ACE-Asia) submicron aerosol types, J. Geophys. Res.-Atmos., 108, 8637, doi:10.1029/2003JD003703, 2003.

McNaughton, C. S., Clarke, A. D., Howell, S. G., et al.: Results from the DC-8 Inlet Characterization Experiment (DICE): Airborne versus surface sampling of mineral dust and sea salt aerosols, Aerosol Sci. Technol., 41, 136–159, doi:10.1080/02786820601118406, 2007.

Middlebrook, A. M., Murphy, D. M., and Thomson, D. S.: Observations of organic material in individual marine particles at Cape Grim during the First Aerosol Characterization Experiment (ACE 1), J. Geophys. Res.-Atmos., 103, 16475–16483, 1998.

Modinia R. L., Graham J. R., Congrong H., Zoran R. D., Observation of the suppression of water uptake by marine particles, Atmos. Res., doi:10.1016/j.atmosres.2010.03.025, in press, 2010.

Novakov, T., Corrigan, C. E., Penner, J. E., et al.: Organic aerosols in the Caribbean trade winds: A natural source?, J. Geophys. Res.-Atmos., 102, 21307–21313, 1997.

Petters, M. D. and Kreidenweis, S. M.: A single parameter representation of hygroscopic growth and cloud condensation nucleus activity, Atmos. Chem. Phys., 7, 1961–1971, doi:10.5194/acp-7-1961-2007, 2007.

Phinney L., Leaitch W. R., Lohmann U., et al., Characterization of the aerosol over the sub-arctic north east Pacific Ocean, Deep-Sea Res., 53, 2410–2433, 2006.

Quinn, P. K., Bates, T. S., Baynard, T., et al.: Impact of particulate organic matter on the relative humidity dependence of light scattering: A simplified parameterization, Geophys. Res. Lett., 32, L22809, doi:10.1029/2005gl024322, 2005.

Raatikainen, T., Vaattovaara, P., Tiitta, P., Miettinen, P., Rautiainen, J., Ehn, M., Kulmala, M., Laaksonen, A., and Worsnop, D. R.: Physicochemical properties and origin of organic groups detected in boreal forest using an aerosol mass spectrometer, Atmos. Chem. Phys., 10, 2063–2077, doi:10.5194/acp-10-2063-2010, 2010.

Roberts, G., Mauger, G., Hadley, O., et al.: North American and Asian aerosols over the eastern Pacific Ocean and their role in regulating cloud condensation nuclei, J. Geophys. Res.-Atmos., 111, D13205, doi:10.1029/2005jd006661, 2006.

Roberts, G. C., Artaxo, P., Zhou, J. C., et al.: Sensitivity of CCN spectra on chemical and physical properties of aerosol: A case study from the Amazon Basin, J. Geophys. Res.-Atmos., 107, 8070, doi:10.1029/2001jd000583, 2002.

Roberts, G. C., and Nenes, A.: A continuous-flow streamwise thermal-gradient CCN chamber for atmospheric measurements, Aerosol Sci. Technol., 39, 206–221, 2005.

Rose, D., Gunthe, S. S., Mikhailov, E., Frank, G. P., Dusek, U., Andreae, M. O., and Pöschl, U.: Calibration and measurement uncertainties of a continuous-flow cloud condensation nuclei counter (DMT-CCNC): CCN activation of ammonium sulfate and sodium chloride aerosol particles in theory and experiment, Atmos. Chem. Phys., 8, 1153–1179, doi:10.5194/acp-8-1153-2008, 2008.

Rose, D., Nowak, A., Achtert, P., Wiedensohler, A., Hu, M., Shao, M., Zhang, Y., Andreae, M. O., and Pöschl, U.: Cloud condensation nuclei in polluted air and biomass burning smoke near the mega-city Guangzhou, China – Part 1: Size-resolved measurements and implications for the modeling of aerosol particle hygroscopicity and CCN activity, Atmos. Chem. Phys., 10, 3365–3383, doi:10.5194/acp-10-3365-2010, 2010.

Russell, L. M., Lenschow, D. H., Laursen, K. K., et al.: Bidirectional mixing in an ACE 1 marine boundary layer overlain by a second turbulent layer, J. Geophys. Res.-Atmos., 103, 16411–16432, 1998.

Russell, L. M., Maria, S. F., and Myneni, S. C. B.: Mapping organic coatings on atmospheric particles, Geophys. Res. Lett., 29, 1779, doi:10.1029/2002GL014874, 2002.

Russell, L. M., Hawkins, L., Frossard, A., et al.: Carbohydrate-like composition of submicron atmospheric particles and their production from ocean bubble bursting, P. Natl. Acad. Sci. USA, 107(15), 6652–6657, 2010.

Shantz, N. C., Leaitch, W. R., Phinney, L., Mozurkewich, M., and Toom-Sauntry, D.: The effect of organic compounds on the growth rate of cloud droplets in marine and forest settings, Atmos. Chem. Phys., 8, 5869–5887, doi:10.5194/acp-8-5869-2008, 2008.

Shinozuka, Y., Clarke, A. D., DeCarlo, P. F., Jimenez, J. L., Dunlea, E. J., Roberts, G. C., Tomlinson, J. M., Collins, D. R., Howell, S. G., Kapustin, V. N., McNaughton, C. S., and Zhou, J.: Aerosol optical properties relevant to regional remote sensing of CCN activity and links to their organic mass fraction: airborne observations over Central Mexico and the US West Coast during MILAGRO/INTEX-B, Atmos. Chem. Phys., 9, 6727–6742, doi:10.5194/acp-9-6727-2009, 2009.

Shulman, M. L., Jacobson, M. C., Charlson, R. J., et al.: Dissolution behavior and surface tension effects of organic compounds in nucleating cloud droplets, Geophys. Res. Lett., 23, 603–603, 1996.

Singh, H. B., Brune, W. H., Crawford, J. H., Flocke, F., and Jacob, D. J.: Chemistry and transport of pollution over the Gulf of Mexico and the Pacific: spring 2006 INTEX-B campaign overview and first results, Atmos. Chem. Phys., 9, 2301–2318, doi:10.5194/acp-9-2301-2009, 2009.

Stith, J. L., Ramanathan, V., Cooper, W. A., et al.: An overview of aircraft observations from the Pacific Dust Experiment campaign, J. Geophys. Res.-Atmos., 114, D05207, doi:10.1029/2008JD010924, 2009.

Subramanian, R., Kok, G. L., Baumgardner, D., Clarke, A., Shinozuka, Y., Campos, T. L., Heizer, C. G., Stephens, B. B., de Foy, B., Voss, P. B., and Zaveri, R. A.: Black carbon over Mexico: the effect of atmospheric transport on mixing state, mass absorption cross-section, and BC/CO ratios, Atmos. Chem. Phys., 10, 219–237, doi:10.5194/acp-10-219-2010, 2010.

Sullivan, R. C., Moore, M. J. K., Petters, M. D., Kreidenweis, S. M., Roberts, G. C., and Prather, K. A.: Effect of chemical mixing state on the hygroscopicity and cloud nucleation properties of calcium mineral dust particles, Atmos. Chem. Phys., 9, 3303–3316, doi:10.5194/acp-9-3303-2009, 2009.

Swietlicki, E., Hansson, H. C., Hameri, K., et al.: Hygroscopic properties of submicrometer atmospheric aerosol particles measured with H-TDMA instruments in various environments - a review, Tellus B, Chem. Phys. Meteorol., 60, 432–469, doi:10.1111/j.1600-0889.2008.00350.x, 2008.

Takahama, S., Gilardoni, S., Russell, L. M., et al.: Classification of multiple types of organic carbon composition in atmospheric particles by scanning transmission X-ray microscopy analysis, Atmos. Environ., 41, 9435–9451, doi:10.1016/j.atmosenv.2007.08.051, 2007.

Tomlinson, J. M., Runjun, L., and Collins, D. R.: Physical and chemical properties of the aerosol within the southeastern Pacific marine boundary layer, J. Geophys. Res.-Atmos., 1–13,

doi:10.1029/2006jd007771, 2007.

Vestin, A., Rissler, J., Swietlicki, E., et al.: Cloud-nucleating properties of the Amazonian biomass burning aerosol: Cloud condensation nuclei measurements and modeling, J. Geophys. Res.-Atmos., 112, D14201, doi:10.1029/2006jd8104, 2007.

Wang, J., Lee, Y.-N., Daum, P. H., Jayne, J., and Alexander, M. L.: Effects of aerosol organics on cloud condensation nucleus (CCN) concentration and first indirect aerosol effect, Atmos. Chem. Phys., 8, 6325–6339, doi:10.5194/acp-8-6325-2008, 2008.

Zhou, J. C., Swietlicki, E., Hansson, H. C., et al.: Submicrometer aerosol particle size distribution and hygroscopic growth measured in the Amazon rain forest during the wet season, J. Geophys. Res.-Atmos., 107, 8055, doi:10.1029/2000jd000203, 2002.